This is a preprint version of

Maintaining Robot Localizability With Bayesian Cramér-Rao Lower Bounds

Accepted at the IEEE/RSJ IROS 2022 conference held in Kyoto, Japan.

The final version will be soon available in my author page https://ieeexplore.ieee.org/author/37086933423

Maintaining Robot Localizability with Bayesian Cramér-Rao Lower Bounds

Justin Cano[1,3], Corentin Chauffaut[2], Eric Chaumette[3], Gaël Pages[3] and Jerome Le Ny[1]

***Abstract*— Accurate and real-time position estimates are crucial for mobile robots. This work focuses on ranging-based positioning systems, which rely on distance measurements between known points, called anchors, and a tag to localize. The topology of the network formed by the anchors strongly influences the tag's localizability, *i.e.,* its ability to be accurately localized. Here, the tag and some anchors are supposed to be carried by robots, which allows enhancing the positioning accuracy by planning the anchors' motions. We leverage Bayesian Cramér-Rao Lower Bounds (CRLBs) on the estimates' covariance in order to quantify the tag's localizability. This class of CRLBs can capture prior information on the tag's position and take it into account when deploying the anchors. We propose a method to decrease a potential function based on the Bayesian CRLB in order to maintain the localizability of the tag while having some prior knowledge about its position distribution. Then, we present a new experiment highlighting the link between the localizability potential and the precision expected in practice. Finally, two real-time anchor motion planners are demonstrated with ranging measurements in the presence or absence of prior information about the tag's position.**

I. Introduction

Mobile robots require reliable, energy-efficient and real-time positioning systems to operate. Various technologies can be used to estimate the position of a robot : computer vision [1] or Global Navigation Satellite Systems (GNSS) [2] are among the leading ones. However, irrespective of the positioning system, an extrinsic measurement is required to determine the bodies' locations in a given frame [2], [3].

We focus on ranging-based localization, which determines positions thanks to distance measurements between the robot to locate, called *tag*, and known reference points, called *anchors*. For our experiments we use Ultra-Wide Band (UWB) sensors, which are increasingly popular in mobile robotics, due to their low cost and energy consumption [4], [5]. In particular, signal Time-of-Flight (ToF) estimation techniques applied to UWB allows up-to-decimeter ranging accuracy [3], [6]–[8], which makes the technology suitable for indoor navigation.

Even with small ranging uncertainties, the geometry of the anchors' network strongly influences the *localizability* of the tags, i.e., their ability to be accurately localized [9].

*This work was supported by FRQNT under grant 2018-PR-253646, by NSERC under grant RGPIN-5287-2018 and by the DGA/AID project 2019.65.0068.00.470.75.01.

[1] J. Cano and J. Le Ny are with the department of Electrical Engineering, Polytechnique Montréal and with GERAD, Montréal, QC, Canada. {justin.cano,jerome.le-ny}@polymtl.ca

[2] C. Chauffaut is with the DISC, ISAE-Supaéro, Toulouse, France corentin.chauffaut@isae-supaero.fr

[3] J. Cano, E. Chaumette and G. Pages are with the DEOS, ISAE-Supaéro, France {gael.pages,eric.chaumette}@isae-suparero.fr

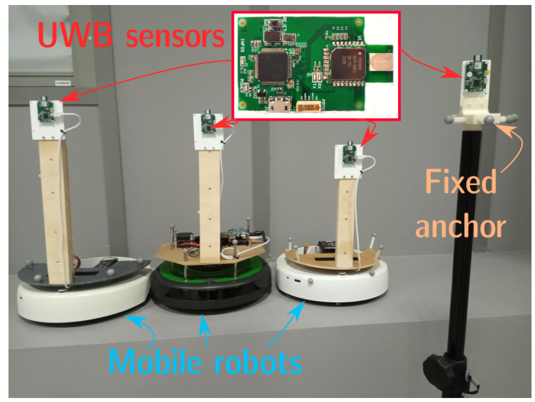

Fig. 1: Robots, fixed anchor and UWB sensors used in the experiments.

This phenomenon is known as *Dilution of Precision* (DoP) in the GNSS literature [2], [10, Chap. 7] and transferable to mobile robotics. To quantify these uncertainties over the tag's location, the *Cramér-Rao Lower Bound* (CRLB), is commonly used as a performance metric for localization systems [9], [11], [12]. The CRLB is a lower bound on covariance that permits computing optimal theoretical performance of estimators independently of their implementation [13], [14].

We assume that some anchors are carried by robots and can be deployed to enhance the tag's *localizability*. This property can be used to design motion planning algorithms, defining a CRLB-based localizability *potential* (*i.e.*, cost function) to decrease in order to improve the tag's positioning accuracy [15]. In previous work [16], we proposed decentralized techniques to optimize localizability in Multi-Robots Systems (MRS) and for robots carrying several tags [17]. The recent work [12] proposes to implement localizability constraints in graph-based planners to enhance the MRS positioning performance. However, these methods requires tag positions that can only been available through estimates.

In this paper, we present an experimental implementation of a motion planner proposed in [16] for an MRS that uses tag position estimates as input. Moreover, we define a novel criterion of localizability, taking into account prior information on the tag's position. Indeed, information on the position distribution can be obtained during the estimation of the tag's position, *e.g.*, using Kalman Filtering. This additional information is considered when modeling localizability, since it directly relates to the estimates' accuracy. To do so, we leverage Bayesian Cramér-Rao Lower Bounds [14]. We also propose a motion planner to improve this bound in real-time and test it in an MRS deployment experiment.

II. Problem Statement

Consider a set $\mathcal{K}$ of K *anchors*, with known positions. The anchors aim to localize a *tag* T, which is a sensor carried by a robot with unknown position $\mathbf{p}_{\mathcal{U}} \in \mathbb{R}^n$, where $n \in \{2,3\}$. The tag performs with each anchor $i \in \mathcal{K}$ noisy distance measurements $\tilde{d}_i$ of $d_i = ||\mathbf{p}_{\mathcal{U}} - \mathbf{p}_i||$ where $\mathbf{p}_i \in \mathbb{R}^n$ denotes i's position. Then an estimate of $\hat{\mathbf{p}}_{\mathcal{U}}$ is computed using the information brought by these measurements. We assume that there exists a subset $\mathcal{K}_M \subseteq \mathcal{K}$ of K_M *mobile anchors* in $\mathbb{R}^n$, each carried by a different robot.

Since the geometry of $\mathcal{K}$ strongly influences the quality of $\hat{\mathbf{p}}_{\mathcal{U}}$, our goal is to design motion planners for $\mathcal{K}_M$ in order to maintain an adequate localizability of T while its carrier performs tasks. First, we model the amount of information brought by the observations $\tilde{\mathbf{d}}$ used to build $\hat{\mathbf{p}}_{\mathcal{U}}$. This approach leverages *Fisher Information Matrices* (FIM) for deterministic parameter $\mathbf{p}_{\mathcal{U}}$ estimation as seen in [9]. Second, we consider that prior information on $\mathbf{p}_{\mathcal{U}}$ is available and used in the estimation process. We assume that the prior on the position is actualized by its estimator that gathers range measurements during the tag trajectory. In particular, we focus on the case of the popular *Kalman Filter* (KF) that dynamically provides a Gaussian model to quantify its estimates' uncertainties. Here, we propose to incorporate this new information in the localizability evaluation thanks to the *Bayesian Fisher Information Matrix* (BFIM). In Section III, we give its definition and a methodology to compute it.

In order to deploy $\mathcal{K}_M$, we design in Section IV a *localizability potential* $J_C(\mathbf{p}_{\mathcal{K}_M}, \mathbf{p}_{\mathcal{U}})$, where $\mathbf{p}_{\mathcal{K}_M} \in \mathbb{R}^{nK_M}$ contains all the positions of $\mathcal{K}_M$. Based on the the BFIM, this potential models the expected precision of the estimates, *i.e.*, J_C increases when the quality of $\hat{\mathbf{p}}_{\mathcal{U}}$ decreases. This yields a minimization problem to deploy $\mathcal{K}_M$ towards an optimal configuration $\mathbf{p}^*_{\mathcal{K}_M}$ that minimizes J_C for a given $\mathbf{p}_{\mathcal{U}}$. We also provide an experiment that highlights the relation between $\hat{\mathbf{p}}_{\mathcal{U}}$ precision and this potential.

Section V presents motion planners for $\mathcal{K}_M$ that maintain dynamically tag's localizability in deterministic (*i.e.*, without prior) or Bayesian contexts. We stress that since the tag is moving to perform tasks, each $\mathbf{p}^k_{\mathcal{U}}$ at time k yields generally a different optimal anchor placement $\mathbf{p}^{k*}_{\mathcal{K}_M}$. For the Bayesian case, a methodology is provided to decrease J_C if the prior density at time k is Gaussian. These algorithms are then tested on an MRS in Section VI. In these experiments, the tag is being located with the Least Squares (LS) algorithm and the KF respectively, using the estimates $\hat{\mathbf{p}}_{\mathcal{U}}$ in the motion planning process.

III. Information Modeling

We aim to quantify the information provided by the measurements and a (possible) prior on $\mathbf{p}_{\mathcal{U}}$. First, we define the FIM and relate it to the uncertainty on $\hat{\mathbf{p}}_{\mathcal{U}}$. Then, we propose methods to evaluate it numerically.

A. Cramér-Rao Lower Bound

Consider the Probability Density Function (PDF) of the prior $\mathbf{p}_{\mathcal{U}}$ on $\mathbf{p}_{\mathcal{U}}$ denoted $f_\pi : \mathbb{R}^n \mapsto \mathbb{R}^+, \mathbf{p}_{\mathcal{U}} \to f_\pi(\mathbf{p}_{\mathcal{U}})$. We have $f_\mu : \mathbb{R}^{Kn} \mapsto \mathbb{R}^+, \tilde{\mathbf{d}} \to f_\mu(\tilde{\mathbf{d}};\mathbf{p})$ the measurements' PDF, considering the vector $\tilde{\mathbf{d}} = [\dots \tilde{d}_i \dots]^\top$ with $i \in \mathcal{K}$ gathering the observations and the vector $\mathbf{p} = [\dots \mathbf{p}_i^\top \dots \mathbf{p}_{\mathcal{U}}^\top]^\top$ containing the sensors' positions. We assume that these PDFs are twice continuously differentiable. Under these assumptions the *Bayesian Fisher Information Matrix* (BFIM) [14] of $\mathbf{p}_{\mathcal{U}}$ is defined as follows

$$\mathbf{F}_B(\mathbf{p}) = -\mathbb{E}_{\mathbf{p}_{\mathcal{U}},\tilde{\mathbf{d}}}\left\{\frac{\partial^2 \ln f_\mu(\tilde{\mathbf{d}};\mathbf{p})}{\partial \mathbf{p}_{\mathcal{U}} \partial \mathbf{p}_{\mathcal{U}}^\top}\right\} - \mathbb{E}_{\mathbf{p}_{\mathcal{U}}}\left\{\frac{\partial^2 \ln f_\pi(\mathbf{p}_{\mathcal{U}})}{\partial \mathbf{p}_{\mathcal{U}} \partial \mathbf{p}_{\mathcal{U}}^\top}\right\} \tag{1}$$

where $\partial^2 f_\bullet / \left(\partial \mathbf{p}_{\mathcal{U}} \partial \mathbf{p}_{\mathcal{U}}^\top\right)$ defines the Hessian matrix of $f_\bullet$ with respect to $\mathbf{p}_{\mathcal{U}}$. If f_π is unknown, (1) is simplified and yields the *Deterministic Fisher Information Matrix* (DFIM)

$$\mathbf{F}_D(\mathbf{p}) := -\mathbb{E}_{\tilde{\mathbf{d}}}\left\{\frac{\partial^2 \ln f_\mu(\tilde{\mathbf{d}};\mathbf{p})}{\partial \mathbf{p}_{\mathcal{U}} \partial \mathbf{p}_{\mathcal{U}}^\top}\right\}, \tag{2}$$

that only depends on the rang measurements distribution.

Theorem 1 (Cramér-Rao Lower Bound [14]): If the BFIM is invertible then the estimator's covariance satisfies

$$\Sigma_{\hat{\mathbf{p}}_{\mathcal{U}}} := \mathbb{E}\left\{(\hat{\mathbf{p}}_{\mathcal{U}} - \mathbf{p}_{\mathcal{U}})(\hat{\mathbf{p}}_{\mathcal{U}} - \mathbf{p}_{\mathcal{U}})^\top\right\} \succeq \mathbf{F}_B^{-1}(\mathbf{p}),$$

where the notation $\mathbf{A} \succeq \mathbf{B}$ denotes that $\mathbf{A} - \mathbf{B}$ is positive semi-definite for $\mathbf{A}$ and $\mathbf{B}$ symmetric. In the case of an invertible DFIM $\mathbf{F}_D$, if $\mathbb{E}\{\hat{\mathbf{p}}_{\mathcal{U}}\} = \mathbf{p}_{\mathcal{U}}$, then $\Sigma_{\hat{\mathbf{p}}_{\mathcal{U}}} \succeq \mathbf{F}_D^{-1}$.

This result is known as the *Cramér-Rao Lower Bound* (CRLB) and we use it as a proxy to quantify the tag's localizability. This performance bound has the advantage to be an explicit function of $\mathbf{p}$. It can be decreased by moving $\mathcal{K}_M$ and is quickly calculable, as shown in the rest of this section.

B. Computation of the DFIM

We assume that the distance observations $\tilde{\mathbf{d}}$ are Gaussian and independent which is common when modeling ToF-based range measurements [3], [9]. Thus we have $\tilde{\mathbf{d}} \sim \mathcal{N}(\mathbf{d}, \mathbf{\Sigma}_d)$, denoting $\mathbf{d} = [\dots d_i^\top \dots] \in \mathbb{R}^K$ and $\mathbf{\Sigma}_d = \mathrm{diag}(\dots \sigma_i^2 \dots) \in \mathbb{R}^{K\times K}$. To compute the DFIM, we use the Slepian Bangs Formula (SBF) for real Gaussian distributions.

Proposition 1 (Slepian-Bangs Formula [13]): Consider a position vector $\mathbf{p}_{\mathcal{U}} = [x,y,z]^\top$ (resp. $\mathbf{p}_{\mathcal{U}} = [x,y]^\top$) that parameterizes the PDF f_g of a Gaussian random vector $\mathbf{g} \sim \mathcal{N}(\bar{\mathbf{g}}(\mathbf{p}_{\mathcal{U}}), \mathbf{\Sigma}_g(\mathbf{p}_{\mathcal{U}}))$, with $\bar{\mathbf{g}} \in \mathbb{R}^K$ and $\mathbf{\Sigma}_g \in \mathbb{R}^{K\times K}$ for some $K \in \mathbb{N}$. Then, the coefficients $F^{\xi,\eta} = -\mathbb{E}_{\mathbf{g}}\left\{\partial^2 \ln f_g / \partial\xi\partial\eta\right\}$ of the DFIM $\mathbf{F}_g \in \mathbb{R}^{n\times n}$ of $\mathbf{g}$ with respect to $\mathbf{p}_{\mathcal{U}}$ coordinates are given as follows

$$F_g^{\xi,\eta} = \frac{\partial \bar{\mathbf{g}}}{\partial \xi}\mathbf{\Sigma}_g^{-1}\frac{\partial \bar{\mathbf{g}}}{\partial \eta} + \frac{1}{2}\mathrm{Tr}\left\{\mathbf{\Sigma}_g^{-1}\frac{\partial \mathbf{\Sigma}_g}{\partial \xi}\mathbf{\Sigma}_g^{-1}\frac{\partial \mathbf{\Sigma}_g}{\partial \eta}\right\},$$

where $\eta, \xi \in \{x,y,z\}$ if $n=3$ (and $\eta,\xi \in \{x,y\}$ if $n=2$).

Since $\partial d_i / \partial \xi = (\xi - \xi_i)/d_i$ for a given coordinate $\xi \in \{x,y,z\}$ and $\mathbf{\Sigma}_d$ is assumed independent of the position, the application of the SBF yields [9]

$$\mathbf{F}_D(\mathbf{p}_{\mathcal{K}}, \mathbf{p}_{\mathcal{U}}) = \sum_{i\in\mathcal{K}} \frac{1}{d_i^2 \sigma_i^2}(\mathbf{p}_{\mathcal{U}} - \mathbf{p}_i)(\mathbf{p}_{\mathcal{U}} - \mathbf{p}_i)^\top, \tag{3}$$

where $\mathbf{p}_{\mathcal{K}} = [\dots \mathbf{p}_i^\top \dots]^\top$ contains the anchors' i positions. The equation (3) clearly indicates that the estimates' quality depends on the tag's *relative positions* (RP) $\mathbf{e}_i := \mathbf{p}_{\mathcal{U}} - \mathbf{p}_i$ with respect to the anchors i. The CRLB exists over a simple condition on the RPs presented below.

Proposition 2: $\mathbf{F}_D$ is invertible if and only if n relative position vectors $\mathbf{e}_i$, $i \in \mathcal{K}$ span $\mathbb{R}^n$.

Proof: We gather the RPs $\mathbf{e}_i$ in $\mathbf{E} = [\dots \mathbf{e}_i \dots] \in \mathbb{R}^{n \times K}$ from (3) and note that $\mathbf{F}_D = \mathbf{E}\mathbf{Q}\mathbf{E}^\top$, with $\mathbf{Q} = \mathrm{diag}(\dots d_i^{-2}\sigma_i^{-2} \dots)$ a invertible diagonal matrix. Then, noting that $\mathrm{rank}(\mathbf{F}_D) = \mathrm{rank}(\mathbf{E})$ fulfills the proof. ■

C. BFIM Computation with Gaussian Prior

Before deployment, the tag might know with some uncertainty its initial position, *e.g.*, we assume that it lies in the operating zone. However, the tag moves to fulfill its task and the prior uncertainty can be propagated through time while updating the distance measurements. Here, we suppose that a distribution is provided by the estimator of $\mathbf{p}_{\mathcal{U}}$ and can be used in order to compute the BFIM over time. Typically, if a KF estimator is used to locate the tag, it yields at each time k the estimate $\hat{\mathbf{p}}_{\mathcal{U}}^k$ and its estimated covariance matrix $\hat{\mathbf{\Sigma}}_{\mathbf{p}_{\mathcal{U}}}^k$ [13]. We assume that the PDF f_π of the prior on $\mathbf{p}_{\mathcal{U}}$ is the Gaussian distribution $\mathcal{N}(\mathbf{p}_{\mathcal{U}}, \mathbf{\Sigma})$ with $\mathbf{\Sigma}$ a given definite positive matrix. Thanks to the SBF, we compute $\mathbb{E}_{\mathbf{p}_{\mathcal{U}}}\left\{\partial^2 \ln f_\pi(\mathbf{p}_{\mathcal{U}}) / \left(\partial \mathbf{p}_{\mathcal{U}} \partial \mathbf{p}_{\mathcal{U}}^\top\right)\right\} = -\mathbf{\Sigma}^{-1}$ and finally (1) becomes

$$\mathbf{F}_B(\mathbf{p}) = \mathbb{E}_{\mathbf{p}_{\mathcal{U}}}\left\{\mathbf{F}_D(\mathbf{p}_{\mathcal{K}}, \mathbf{p}_{\mathcal{U}})\right\} + \mathbf{\Sigma}^{-1}. \quad (4)$$

Then, we need to evaluate $\mathbb{E}_{\mathbf{p}_{\mathcal{U}}}\left\{\mathbf{F}_D(\mathbf{p}_{\mathcal{K}}, \mathbf{p}_{\mathcal{U}})\right\}$ which is not analytically possible in general. However, we can approximately evaluate it thanks to the *unscented transform algorithm* [18, Chap. 5], which is a standard approach to sample random Gaussian distributions. To do so, we compute $\mathbf{R} := [\mathbf{r}_1 \dots \mathbf{r}_n]$ the generalized square root of $\mathbf{\Sigma}$ *i.e.*, which fulfills $\mathbf{\Sigma} = \mathbf{R}^\top\mathbf{R}$. Then, we form the set of sampling points

$$\mathcal{S} = \{\mathbf{p}_{\mathcal{U}}\} \cup_{i=1}^n \{\mathbf{p}_{\mathcal{U}} + \delta\mathbf{r}_i, \mathbf{p}_{\mathcal{U}} - \delta\mathbf{r}_i\},$$

where $\eta = \delta\sqrt{n+\beta}$ is parameterized with some constants $\alpha, \beta > 0$. Finally, this expectation can be approximated with

$$\mathbb{E}_{\mathbf{p}_{\mathcal{U}}}\left\{\mathbf{F}_D(\mathbf{p}_{\mathcal{K}}, \mathbf{p}_{\mathcal{U}})\right\} \approx \sum_{\mathbf{y}_j \in \mathcal{S}} w_\pi(\mathbf{y}_j)\mathbf{F}_D(\mathbf{p}_{\mathcal{K}}, \mathbf{y}_j) \quad (5)$$

where $w(\mathbf{y}_j) = f_\pi(\mathbf{y}_j) / \sum_{l \in \mathcal{S}} f_\pi(\mathbf{y}_l)$. The scheme (5) provides a computationally efficient estimate $\hat{\mathbf{F}}_B$ of $\mathbf{F}_B$, which can be implemented in real-time.

IV. Localizability Potential

Here, we design a localizability potential that permits $\mathcal{K}_M$ deployment. Then an experiment that illustrates the link between empirical localizability and its potential is provided.

A. Localizability Potential

We aim to design motion planners that enhance the quality of $\hat{\mathbf{p}}_{\mathcal{U}}$. We use LS and the KF estimators to compute these estimates. These algorithms are designed to minimize the total Mean Square Error (MSE) of $\hat{\mathbf{p}}_{\mathcal{U}}$, defined as follows

$$MSE(\hat{\mathbf{p}}_{\mathcal{U}}) := \mathbb{E}\left\{||\hat{\mathbf{p}}_{\mathcal{U}} - \mathbf{p}_{\mathcal{U}}||^2\right\} = \mathrm{Tr}\left\{\Sigma_{\hat{\mathbf{p}}_{\mathcal{U}}}\right\}.$$

Thus, we choose the MSE as performance criterion on the estimates to quantify the tag's localizability. The CRLB, defined in the Theorem 1, yields the following result for each considered FIM, $C \in \{D, B\}$ depending with respect to which information we condition

$$J_C(\mathbf{p}_{\mathcal{K}_M}, \mathbf{p}_{\mathcal{U}}) := \mathrm{Tr}\left\{\mathbf{F}_C^{-1}(\mathbf{p})\right\} \leq MSE(\hat{\mathbf{p}}_{\mathcal{U}}), \quad (6)$$

where $J_C(\mathbf{p}_{\mathcal{K}_M}, \mathbf{p}_{\mathcal{U}})$ is the *localizability potential* and with $\mathbf{p}_{\mathcal{K}_M} := [\dots, \mathbf{p}_i^\top, \dots]^\top$ for $i \in \mathcal{K}_M$. Then, *we assume* that decreasing J_C yields a better MSE for the estimator $\hat{\mathbf{p}}_{\mathcal{U}}$ in practice [9], [12]. Hence, we define the following placement problem for the mobile anchors

$$\mathbf{p}_{\mathcal{K}_M}^* = \underset{\mathbf{p}_{\mathcal{K}_M} \in \mathbb{R}^{nK_M}}{\mathrm{argmin}} \; J_C(\mathbf{p}_{\mathcal{K}_M}, \mathbf{p}_{\mathcal{U}}) \quad (7)$$

where $\mathbf{p}_{\mathcal{K}_M}^*$ depends on the tag's position. We propose to solve (7) locally in real-time by descending the potential gradient, which is a common approach for mobile robot motion planning [19]. We compute the partial derivatives of J_C, with respect to $\xi_i \in \{x_i, y_i, z_i\}$ a given coordinate of $i \in \mathcal{K}$, thanks to the following formula [15]

$$\frac{\partial J_C(\mathbf{p}_{\mathcal{K}_M}, \mathbf{p}_{\mathcal{U}})}{\partial \xi_i} = -\mathrm{Tr}\left\{\mathbf{F}_C^{-2}\frac{\partial \mathbf{F}_C}{\partial \xi_i}\right\}, C \in \{D, B\}. \quad (8)$$

Then, the results of (8) are gathered in gradient vectors $\nabla_i J_C(\mathbf{p}_{\mathcal{K}_M}, \mathbf{p}_{\mathcal{U}}) := [\partial J_C(\mathbf{p}_{\mathcal{K}_M}, \mathbf{p}_{\mathcal{U}}) / \partial \mathbf{p}_i]^\top \in \mathbb{R}^n$ for each $i \in \mathcal{K}_M$, which yields the total gradient $\nabla J_C(\mathbf{p}_{\mathcal{K}_M}, \mathbf{p}_{\mathcal{U}}) = [\dots \nabla_i J_C^\top(\mathbf{p}_{\mathcal{K}_M}, \mathbf{p}_{\mathcal{U}}) \dots]^\top \in \mathbb{R}^{nK_M}$ for the set $\mathcal{K}_M$. The differentiation of the DFIM defined in (3), required to evaluate the gradient of J_D with (8), gives

$$\frac{\partial \mathbf{F}_D}{\partial \xi_i} = \frac{1}{\sigma_i^2}\left(\frac{2(\xi - \xi_i)}{d_i^4}\mathbf{e}_i\mathbf{e}_i^\top + \frac{1}{d_i^2}\mathbf{D}_{\xi_i}\right), \quad (9)$$

denoting $\xi \in \{x, y, z\}$ the tag' coordinates. $\mathbf{D}_{\xi_i} \in \mathbb{R}^{n \times n}$ is obtained using elementary differentiation rules

$$D_{\xi_i}^{\eta,\zeta} = \begin{cases} 2(\xi_i - \xi), \text{ if } \eta = \zeta = \xi, \\ \zeta_i - \zeta, \text{ if } \eta = \xi \text{ and } \zeta \neq \xi, \\ 0, \text{ if } \eta \neq \xi \text{ and } \zeta \neq \xi, \end{cases}$$

and $D_{\xi_i}^{\zeta,\eta} = D_{\xi_i}^{\eta,\zeta}$, for all $\eta, \zeta \in \{x, y, z\}^2$.

B. An Example of Localizability Enhancement

We show an example that highlights the dependence between the localizability potential and the estimates' precision through a simple experiment. Consider a localization system made of two fixed anchors $\mathcal{K} = \{K_1, K_2\}$ and a tag, carried by a ground robot shown in Fig. 1. Here, the anchors and the tags are custom boards equipped with a Decawave `DW1000M` UWB module [8]. The anchors are placed on tripods at the

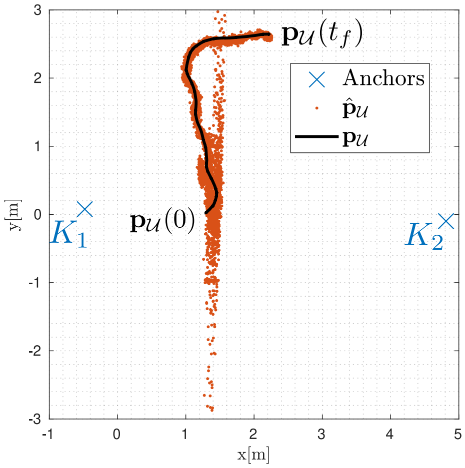

Fig. 2: Estimates $\hat{\mathbf{p}}_{\mathcal{U}}(t)$ and actual trajectory $\mathbf{p}_{\mathcal{U}}(t)$.

same height $z_1 = z_2 = 1.7$ m. We assume that the tag's height $z = 0.7$ m is a known parameter and so $\mathbf{p}_{\mathcal{U}} = [x, y]^\top$ has to be determined through ranging. Each anchor-tag pair $(i, T), i \in \mathcal{K}$ acquires a distance measurement $\tilde{d}_i$ thanks to the bias-compensated *Single-Sided Two-Way Ranging* (SSTWR) protocol described in [6]. These estimates $\hat{\mathbf{p}}_{\mathcal{U}}$ are computed by solving the LS problem

$$\hat{\mathbf{p}}_{\mathcal{U}} = \underset{\mathbf{p}_{\mathcal{U}} \in \mathbb{R}^2}{\text{argmin}} \sum_{i \in \mathcal{K}} \left(\tilde{d}_i - ||\mathbf{p}'_{\mathcal{U}} - \mathbf{p}'_i|| \right)^2 \tag{10}$$

thanks to the Gauss-Newton algorithm [20], where $\mathbf{p}'_{\mathcal{U}} := [\mathbf{p}_{\mathcal{U}}^\top, z]^\top$ and $\mathbf{p}'_i := [\mathbf{p}_i^\top, z_i]^\top$. Here, we assume that the information is modeled by the DFIM $\mathbf{F}_D$ introduced in (2) since we do not provide prior information to build $\hat{\mathbf{p}}_{\mathcal{U}}$. The measurement noise is modeled with a standard deviation of $\sigma = 2.5$ cm. We used a millimeter-accurate motion capture system, which provides a ground truth for $\mathbf{p}_{\mathcal{U}}$, to compute estimation errors.

As shown in Fig. 2, the tag's initial position $\hat{\mathbf{p}}_{\mathcal{U}}(0)$ is almost aligned with the anchors. This configuration has a poor localizability since Proposition 2 states that the DFIM is singular in the case of sensors alignment. To improve this configuration, the robot is deployed following a gradient descent scheme [15] using (8) and (9)

$$\mathbf{p}_{\mathcal{U}}^{k+1} = \mathbf{p}_{\mathcal{U}}^k - \gamma^k \nabla_T J_D(\mathbf{p}_{\mathcal{U}}^k),$$

with $\nabla_T J_D(\mathbf{p}_{\mathcal{U}}^k) = -\sum_{i \in \mathcal{K}} \nabla_i J_D(\mathbf{p}_{\mathcal{U}}^k)$. The superscript k denotes time indices and $\gamma^k > 0$ is a normalized step-size

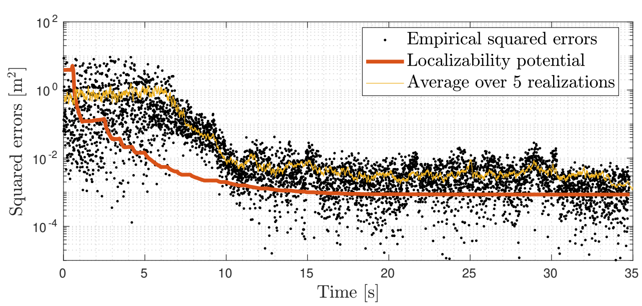

Fig. 3: Localizability function and squared errors.

[20]. We provided the way-points generated by the scheme to a lower-level position controller [21, p.529] using the ground truth values as input. The trajectory is visible in Fig. 2 and superposed with the obtained estimates $\hat{\mathbf{p}}_{\mathcal{U}}$.

In Fig. 3 we plotted the time series of the localizability cost function $J_C(\mathbf{p}_{\mathcal{U}}^k)$ alongside the empirical squared errors $SE^k := ||\hat{\mathbf{p}}_{\mathcal{U}} - \mathbf{p}_{\mathcal{U}}||^2$ for a trajectory realization. As seen in (6), the potential J_D is a lower bound on the expectation of the squared error which seems to be empirically observed along the trajectory after 1 s. To highlight this remark, we plotted a 100-point sliding average curve over 5 trajectories in Fig. 3. This experiment stresses that the descent of the localizability potential has strongly enhanced (SE decreases of three orders of magnitude) the estimates' quality.

V. Motion Planners

In this section, we provide two methods to decrease the localizability potentials J_D and J_B with real-time position estimates.

A. Deterministic Motion Planner

In this subsection we suppose that we do not have access to prior information ,*i.e.*, $\mathbf{p}_{\mathcal{U}}$ is treated as a deterministic parameter and J_D is considered as the potential. To decrease this function, we use the *Deterministic Motion Planner* (DMP) based on the approach presented in [16, V]. This motion planner uses the estimated gradient $\nabla_{\mathbf{p}_{\mathcal{K}_M}} J_c(\mathbf{p}_{\mathcal{K}_M}, \hat{\mathbf{p}}_{\mathcal{U}})$ of $J_c(\mathbf{p}_{\mathcal{K}_M}, \mathbf{p}_{\mathcal{U}})$ where $\mathbf{p}_{\mathcal{U}}$ is replaced by its estimate $\hat{\mathbf{p}}_{\mathcal{U}}$. At each time k, a local variable $\mathbf{q}^{l,k}$ is set to $\mathbf{q}^{0,k} = \mathbf{p}_{\mathcal{K}_M}^k$ in order to perform the following descent operation

$$\mathbf{q}^{l+1,k} = \mathbf{q}^{l,k} - \mathbf{\Gamma}^l \nabla J_D(\mathbf{q}^{l,k}, \hat{\mathbf{p}}_{\mathcal{U}}^k), \tag{11}$$

for $l \in [0, L-1]$ where L is the maximum iterations number. The localizability gradient is evaluated with the last available estimate $\hat{\mathbf{p}}_{\mathcal{U}}^k$. The step-size matrix $\mathbf{\Gamma}^k = \text{diag}(\dots, \gamma_i^k \mathbf{I}_n, \dots)$ is parameterized with $\gamma^l = \gamma_0 \min\{1, \gamma_M ||\nabla_i J_D(\mathbf{q}^l, \hat{\mathbf{p}}_{\mathcal{U}}^k)||^{-1}\}$ where $\gamma_0 > 0$ and γ_M is set order to limit the magnitude of the gradient [20]. The DMP is stopped i) if $\max_i ||\nabla_i J_D(\mathbf{q}^{l,k}, \hat{\mathbf{p}}_{\mathcal{U}}^k)|| < \epsilon$ where $\epsilon > 0$ is a given tolerance; or ii) if L iterations are computed and then yields $\mathbf{p}_{\mathcal{K}_M}^{k,*}$. Finally, $\mathbf{p}_{\mathcal{K}_M}^{k,*}$ is transmitted to the mobile anchors, setting $\mathbf{p}_{\mathcal{K}_M,\text{ref}}^{k+1} := \mathbf{q}^{L,k}$ as the anchors' controller references at time $k+1$.

B. Bayesian Motion Planner

In the case of a Gaussian distribution prior $\mathcal{N}\left(\mathbf{p}_{\mathcal{U}}^k, \Sigma^k\right)$, the information is gathered in the BFIM $\mathbf{F}_B$ given by (1). Here we propose the *Bayesian Motion Planner* (BMP) that decreases an approximated gradient of J_B. We suppose that $\mathbf{\Sigma}^k$ and $\hat{\mathbf{p}}_{\mathcal{U}}^k$ are known by the motion planner at time k. First, the equation (8) used to compute the potential gradient involves the quantity $\mathbf{F}_B^k$ which must be estimated. To do so, we use the numerical approximation (5), that yields $\hat{\mathbf{F}}_B^k$ computed thanks to $\{\hat{\mathbf{p}}_{\mathcal{U}}^k, \mathbf{\Sigma}^k\}$. Second, $\partial \mathbf{F}_B / \partial \xi_i^k$ computation is required for all $\xi_i^k \in \{x_i^k, y_i^k, z_i^k\}$ with $i \in \mathcal{K}_M$ at time k. The computation of $\partial \mathbf{F}_B(\mathbf{p}^k) / \partial \xi_i^k =$

$\partial \mathbb{E}_{\mathbf{p}_{\mathcal{U}}} \left\{ \mathbf{F}_D(\mathbf{p}_{\mathcal{U}}^k, \mathbf{p}_{\mathcal{K}}^k) \right\} / \partial \xi_i^k$ involves an expectation over the prior PDF and cannot be analytically computed.

To address this issue, we implement a stochastic gradient algorithm [22]. The BMP initializes the local variable $\mathbf{q}^{0,k} = \mathbf{p}_{\mathcal{K}_M}^k$ similarly to the DMP. At each iteration l of the algorithm, a random draw $\mathbf{r}^l$ with $\mathbf{r}^l \sim \mathcal{N}\left(\hat{\mathbf{p}}_{\mathcal{U}}^k, \Sigma^k\right)$ is realized. Then for each mobile tag $i \in \mathcal{K}_M$, we compute the following gradient descent step

$$\mathbf{q}_i^{l+1} = \mathbf{q}_i^l - \gamma^l \hat{\nabla}_i J_B^l, \tag{12}$$

where $\hat{\nabla}_i J_B^l = [\dots s_{\xi_i}^l \dots]^\top$, for $\xi \in \{x, y, z\}$ with

$$s_{\xi_i}^l = \mathrm{Tr}\left\{ \left(\hat{\mathbf{F}}_B^l\right)^{-2} \frac{\partial \mathbf{F}_D(\mathbf{q}^l, \mathbf{r}^l)}{\partial \xi_i} \right\},$$

and $\mathbf{q}^l = [\dots \mathbf{q}_i^\top \dots]^\top$. In (12), for a sufficiently small step-size γ^l, we approximate $\partial \mathbb{E}_{\mathbf{p}_{\mathcal{U}}} \left\{ \mathbf{F}_D(\mathbf{p}_{\mathcal{K}}, \mathbf{p}_{\mathcal{U}}) \right\} / \partial \xi_i$ after repeating the iterations. Indeed, performing (12) with small moves empirically averages the gradient by successive draws and then estimates its expectation with a limited computational cost [22]. We adjusted $\mathbf{\Gamma}^l$ with the rule presented in Section V-A in order to compute $\hat{\nabla}_{\mathbf{p}_{\mathcal{K}_M}} J_B(\mathbf{q}^l, \mathbf{r}^l) = [\dots, \hat{\nabla}_i J_B^l, \dots]^\top$, $i \in \mathcal{K}_M$. After L iterations of (12), the BMP transmits $\mathbf{q}^{L,k}$ to the anchors as new reference positions $\mathbf{p}_{\mathcal{K}_M,\mathrm{ref}}^{k+1}$. Algorithm 1 summarizes the procedure.

Input: $\mathbf{p}_{\mathcal{K}}^k$,$\hat{\mathbf{p}}_{\mathcal{U}}^k$,$\mathbf{\Sigma}^k$
$\mathbf{q}^{0,k} = \mathbf{p}_{\mathcal{K}_M}^k$
for $l \in [0, L-1]$ **do**
  draw randomly $\mathbf{r}^l \sim \mathcal{N}\left(\hat{\mathbf{p}}_{\mathcal{U}}^k, \Sigma^k\right)$
  compute $\hat{\mathbf{F}}_B$ with (5)
  compute $\hat{\nabla}_{\mathbf{p}_{\mathcal{K}_M}} J_B(\mathbf{q}^l, \mathbf{r}^l)$ with (12)
  $\mathbf{q}^{l+1,k} = \mathbf{q}^{l,k} - \mathbf{\Gamma}^l \hat{\nabla}_{\mathbf{p}_{\mathcal{K}_M}} J_B(\mathbf{q}^l, \mathbf{r}^l)$
end
transmit $\mathbf{p}_{\mathcal{K}_M,\mathrm{ref}}^{k+1} := \mathbf{q}^{L,k}$ to $\mathcal{K}_M$.

Algorithm 1: BMP algorithm.

VI. Multi-Robot Deployment

We present two deployment experiments using the DMP and the BMP. We consider a system of three anchors $\mathcal{K} = \{K_1, K_2, K_3\}$, with two of them $\mathcal{K}_M = \{K_1, K_2\}$ carried by ground robots (where $z_1 = 43$ cm, $z_2 = 53$ cm) and the third fixed on a tripod ($z_3 = 1.60$ m). We aim to localize a tag T carried by a robot (where $z = 51$ cm is known), with $\mathbf{p}_{\mathcal{U}} \in \mathbb{R}^2$ unknown. The tag's location is determined thanks to range measurements provided by SSTWR performed by UWB sensors, as in Section IV-B. The three robots used in the experiments are shown in Fig. 1.

The tag has an assigned task that involves to follow a given trajectory $\{\mathbf{p}_{\mathcal{U},\mathrm{ref}}^k\}$ along the x-axis of the workspace between the origin and $x(t_f) = 1.5$ m, where t_f is the final time of the experiment. The estimates $\hat{\mathbf{p}}_{\mathcal{U}}$ are used by the tag to perform its own trajectory and by the anchors to decrease the localizability potential. The architecture of the system is summarized in Fig. 4 and is implemented using the middleware `ROS Melodic`.

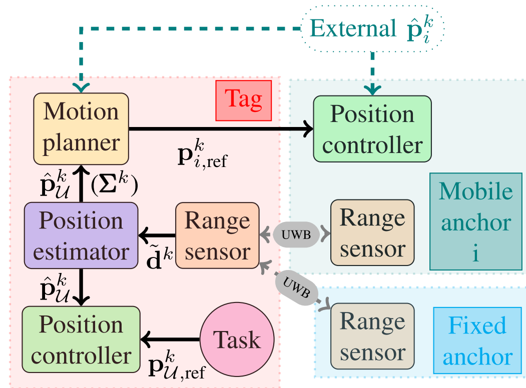

Fig. 4: System architecture.

A. DMP implementation with LS estimator

First, we implemented the DMP using $\hat{\mathbf{p}}_{\mathcal{U}}^k$ obtained by the LS estimator (10) with the last available measurements. The initial positions $\mathbf{p}_j(0)$ of the robots $j \in \mathcal{K}_M \cup \{T\}$ with the fixed anchor's position $\mathbf{p}_3$ are shown in Fig. 5. The DMP computes an iteration when the reference position of the tag $\mathbf{p}_{\mathcal{U},\mathrm{ref}}^k$ and the planed anchors' position $\mathbf{p}_{i,\mathrm{ref}}^k$ are reached for K_1 and K_2 (with a tolerance of 20 cm). After convergence, the DMP sends to the anchors the new reference positions $\mathbf{p}_{i,\mathrm{ref}}^{k+1}$ while $\mathbf{p}_{\mathcal{U},\mathrm{ref}}^{k+1}$ is independently sent to the tag. Then, they are transmitted to the anchors position controllers and processed. After a time of $t_f = 140$ s the robots reached their final positions $\mathbf{p}_j(t_f)$, $j \in \mathcal{K}_M \cup \{T\}$.

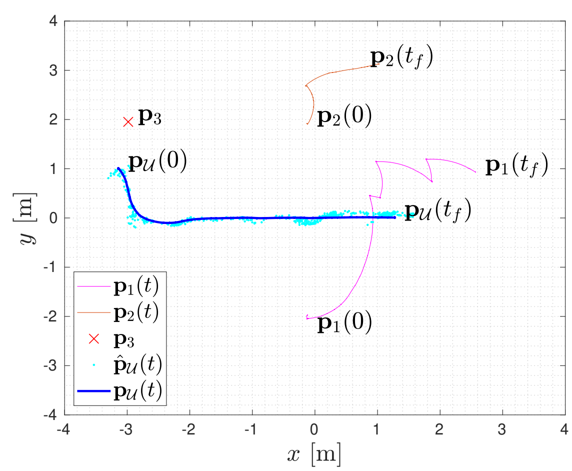

Fig. 5: Robots trajectory and estimates (DMP/LS).

The trajectories of each robot with the estimates $\hat{\mathbf{p}}_{\mathcal{U}}$ are plotted in Fig. 5 and their squared errors (SE) in Fig. 6a. During the trajectory, the average squared error on $\hat{\mathbf{p}}_{\mathcal{U}}$ is around $(0.11)^2$ m, which remains sufficient to follow the tag's reference trajectory. Nevertheless, we noticed some estimation issues due to measurement outliers, produced by nearby reflective surfaces such as the ground and the robots' bodies. This is a strong motivation to consider prior information (*i.e.*, filtering) in the estimation schemes

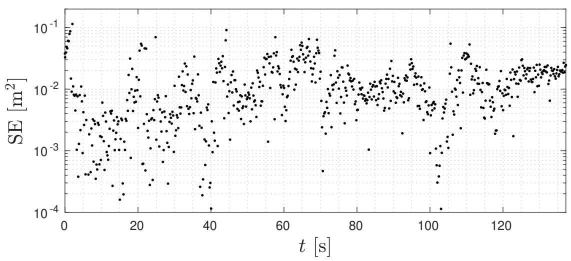

(a) Empirical squared errors.

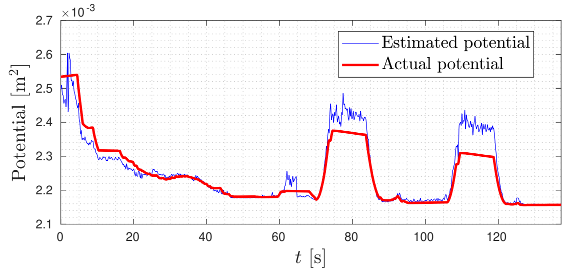

(b) Localizability potential.

Fig. 6: Results with (DMP/LS).

to filter these unmodelized phenomena which can generate significant errors in the localizability gradient computation.

In Fig. 6b we plotted the localizability potential computed with the estimated $\hat{\mathbf{p}}_{\mathcal{U}}$ (*i.e.*, $J_D(\mathbf{p}_{\mathcal{K}_M}, \hat{\mathbf{p}}_{\mathcal{U}})$, in blue) and the reference $\mathbf{p}_{\mathcal{U}}$ (*i.e.*, $J_D(\mathbf{p}_{\mathcal{K}_M}, \mathbf{p}_{\mathcal{U}})$, in red) obtained by the motion capture reference system. The increases in the potential observable at $t = 70$ s and $t = 110$ s are due to the tag deploying faster than the anchors while it achieves its task. Indeed, gradient computations in (11) are based on the $k-1$-th tag's position. However, the potential is decreased after the anchors' deployment and maintained at low values during the trajectory. We remark that the potential values in Fig. 6b are lesser than the SE presented in Fig. 6a since (6) holds.

B. BMP implementation with EKF estimator

Here, we present the BMP-based deployment while an Extended Kalman Filter (EKF) [13] is used to compute $\hat{\mathbf{p}}_{\mathcal{U}}$. In order to implement the EKF, we consider the continuous-time kinematic state $\mathbf{x}(t) = [\mathbf{p}_{\mathcal{U}}, \mathbf{v}_{\mathcal{U}}]^\top$, where $\mathbf{v}_{\mathcal{U}} = [v_x, v_y]^\top$ is the tag velocity vector. We suppose the single-integrator dynamic model as follows for $\xi \in \{x, y\}$

$$\begin{cases} \dot{\xi} = v_\xi + \omega_\xi, \\ \dot{v}_\xi = \kappa_\xi \end{cases}$$

where ω_ξ are κ_ξ independent centered white Gaussian noises with power spectral densities $S_{\omega,\omega} = 10^{-2}$ and $S_{\kappa,\kappa} = 10^{-3}$. The observation model, at time l is given by $\tilde{\mathbf{d}}^l := \mathbf{d}^l + \boldsymbol{\nu}^l$ denoting $\mathbf{d}^l = [d_1, d_2, d_3]^\top$ and $\boldsymbol{\nu}^l \sim \mathcal{N}\left(\mathbf{0}, (0.05)^2\mathbf{I}_3\right)$.

After careful discretization of the tag's kinematics model, we implemented the EKF in the corresponding robot. It allowed to compute estimates $\hat{\mathbf{x}}^l$ and their covariance matrices $\hat{\boldsymbol{\Sigma}}^l_{\mathbf{x}}$ with an average refresh rate of 20 Hz when new

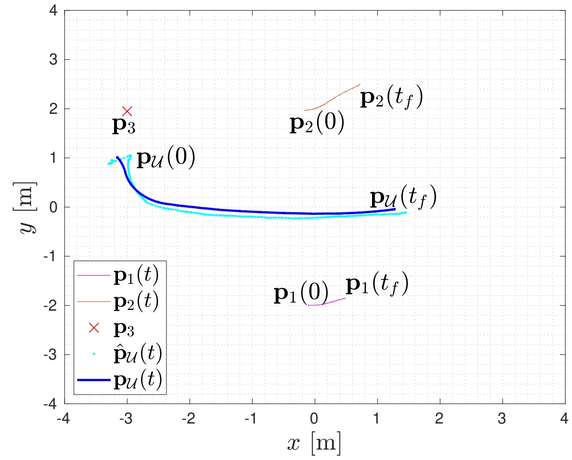

Fig. 7: Robots trajectory and estimates (BMP/EKF).

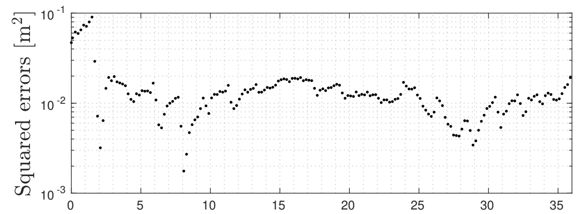

(a) Empirical squared errors.

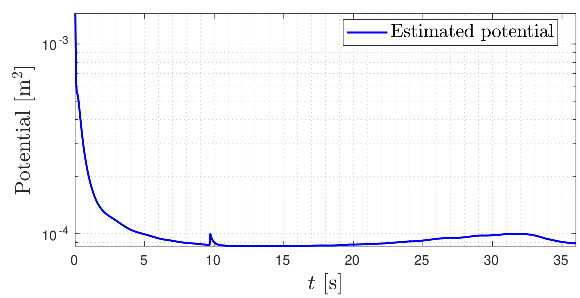

(b) Localizability potential.

Fig. 8: Results with (BMP/EKF).

measurements $\mathbf{d}^l$ are available. We use as input of the BMP at step k the last available estimate $\hat{\mathbf{p}}^k_{\mathcal{U}}$ extracted from $\hat{\mathbf{x}}^k$ and $\boldsymbol{\Sigma}^k := \hat{\boldsymbol{\Sigma}}^k_{\mathbf{p}_{\mathcal{U}}}$ from the estimated covariance $\hat{\boldsymbol{\Sigma}}^k_{\mathbf{x}}$ provided by the EKF. Then, we repeated with the BMP the same experiment presented in VI-A.

For this experiment, the trajectories and the estimates are plotted in Fig. 7 while the SE are shown in Fig. 8a. At the beginning of the trajectory, we observe on Fig. 8a a quick decrease of the SE and the potential function on Fig. 8b. Indeed, the measurement, provided at a 20 Hz refresh rate allows the EKF to converge fast and $\mathrm{Tr}\left\{(\boldsymbol{\Sigma}^k)^{-1}\right\}$ increases as the state estimate's uncertainty decreases. Around $t = 30$ s, we notice a slight increase of the potential values, due to the temporary alignment of the three robots in the workspace. This slight raise yields an insufficient gradient norm to redeploy the anchors (the gradient is strongly weighted by $\mathbf{\Sigma}^k$, which remains low has the EKF has converged) while the estimates remains at tolerable precision. Moreover, int contrast to the experiment presented in Section VI-A, the EKF smoothed the errors generated by measurement outliers despite using a simple kinematic model.

In the BMP experiment, the tag's took $t_f = 36$ s to reach its destination. This difference with DMP is explained by the more restrained deployment of the anchors. Indeed, considering the prior information given by the EKF (which takes into account all measurement history [13]) the localizability is less dependent on the geometry than in the deterministic case. Despite transient effects at the beginning of the experiment due to the EKF convergence, the mean of the SE over the trajectory is $(0.11)^2$ m which yields a similar performance than DMP for a faster deployment time. Indeed, the DMP deploys the anchors at local optimal positions in terms of geometry at each time k irrespective of the prior information used to build $\hat{\mathbf{p}}_k$, which can be time-costly. In contrast, the BMP is influenced dynamically by the prior on $\mathbf{p}_{\mathcal{U}}$ and redeploys the anchors if that information suddenly decreases, which makes it more operative.

VII. Conclusion and Perspectives

In this paper, we showed a method to maintain the localizability of a robot performing relative distance measurements with known positions sensors, *i.e*, anchors. Thanks to covariance inequalities, we defined a novel localizability potential taking into account prior information on the robot's position. We proposed a methodology to compute and optimize this quantity by moving mobile anchors. Through experiment, we highlighted the relationship between the localizability cost function and actual positioning uncertainties. Finally, we validated existing and novel motion planners in multi-robot experiments. Future work will include leveraging tighter bounds capturing more realistic measurement models and prior dynamics.

Acknowledgment

The authors thank Louis Treton from ISAE for his availability and his assistance.

References

[1] P. Corke, *Robotics, Vision and Control*, B. Siciliano and O. Khatib, Eds. Berlin, Heidelberg: Springer Berlin Heidelberg, 2011.

[2] P. D. Groves, *Principles of GNSS, inertial, and multisensor integrated navigation systems*, 2nd ed. Artech House, 2013.

[3] Z. Sahinoglu, S. Gezici, and I. Guvenc, *Ultra-wideband Positioning Systems: Theoretical Limits, Ranging Algorithms, and Protocols*. Cambridge University Press, 2008.

[4] Amanda Prorok, "Models and Algorithms for Ultra-Wideband Localization in Single- and Multi-Robot Systems," Ph.D. dissertation, École Polytechnique Fédérale de Lausanne, Lausanne, 2013.

[5] V. Mai, M. Kamel, M. Krebs, A. Schaffner, D. Meier, L. Paull, and a. R. Siegwart, "Local Positioning System Using UWB Range Measurements for an Unmanned Blimp," *IEEE Robotics and Automation Letters*, vol. 3, no. 4, pp. 2971–2978, Oct. 2018.

[6] J. Cano, G. Pagès, E. Chaumette, and J. Le Ny, "Clock and power-induced bias correction for UWB time-of-flight measurements," *IEEE Robotics and Automation Letters*, vol. 7, no. 2, pp. 2431–2438, 2022.

[7] B. Etzlinger and H. Wymeersch, "Synchronization and Localization in Wireless Networks," *Foundations and Trends in Signal Processing*, vol. 12, pp. 1–106, Jan. 2018.

[8] Decawave, *DW1000 module : datasheet and user manual*, v2.12 ed. Qorvo, 2017, https://www.decawave.com/product/dwm1000-module/.

[9] N. Patwari, J. N. Ash, S. Kyperountas, A. O. Hero, R. L. Moses, and N. S. Correal, "Locating the nodes: cooperative localization in wireless sensor networks," *IEEE Signal Processing Magazine*, vol. 22, no. 4, pp. 54–69, Jul. 2005.

[10] X. Lv, K. Liu, and P. Hu, "Geometry Influence on GDOP in TOA and AOA Positioning Systems," in *2010 Second International Conference on Networks Security, Wireless Communications and Trusted Computing*, vol. 2, Apr. 2010, pp. 58–61.

[11] Z. Liu, W. Chen, Y. Wang, and J. Wang, "Localizability estimation for mobile robots based on probabilistic grid map and its applications to localization," in *2012 IEEE International Conference on Multisensor Fusion and Integration for Intelligent Systems (MFI)*, Sep. 2012, pp. 46–51.

[12] A. Papalia, N. Thumma, and J. Leonard, "Prioritized Planning for Cooperative Range-Only Localization in Multi-Robot Networks," *arXiv:2109.05132 [cs]*, Sep. 2021.

[13] S. M. Kay, *Fundamentals of Statistical Signal Processing: Estimation Theory*. Englewood Cliffs, NJ, USA: Prentice-Hall, 1993.

[14] H. L. Van Trees and K. L. Bell, "Bayesian bounds for parameter estimation and nonlinear filtering/tracking," *AMC*, vol. 10, no. 12, pp. 10–1109, 2007.

[15] J. Le Ny and S. Chauvière, "Localizability-Constrained Deployment of Mobile Robotic Networks with Noisy Range Measurements," in *2018 Annual American Control Conference (ACC)*, Jun. 2018, pp. 2788–2793.

[16] J. Cano and J. Le Ny, "Ranging-Based Localizability-Constrained Deployment of Mobile Robotic Networks," *arXiv:2202.00756 [cs]*, Feb. 2022. [Online]. Available: http://arxiv.org/abs/2202.00756

[17] ——, "Improving Ranging-Based Location Estimation with Rigidity-Constrained CRLB-Based Motion Planning," in *2021 IEEE International Conference on Robotics and Automation (ICRA)*, May 2021, pp. 5758–5764, iSSN: 2577-087X.

[18] S. Sarkka, *Bayesian Filtering and Smoothing*. Cambridge: Cambridge University Press, 2013.

[19] H. Choset, K. Lynch, S. Hutchinson, K. George, W. Burgard, L. Kavraki, and S. Thrun, *Principles of Robot Motion*. Cambridge, Massachusetts: The MIT Press, 2005, vol. 1.

[20] D. P. Bertsekas, *Nonlinear programming*, 3rd ed. Belmont, MA: Athena Scientific, 2016.

[21] K. M. Lynch and F. C. Park, *Modern robotics: mechanics, planning, and control*. Cambridge, UK: Cambridge University Press, 2017, oCLC: ocn983881868.

[22] L. Bottou, "Stochastic gradient descent tricks," in *Neural networks: Tricks of the trade*. Springer, 2012, pp. 421–436.